The Diurnal Cycle of Clouds in Tropical Cyclones
over the Western North Pacific Basin

Kohei Fukuda[1], Kazuaki Yasunaga[1], Ryo Oyama[2, 3], Akiyoshi Wada[3],
Atsushi Hamada[1], and Hironori Fudeyasu[4]

[1]*Department of Earth Science, Graduate School of Science and Engineering, University of Toyama, Toyama, Japan*
[2]*Forecast Division, Forecast Department, Japan Meteorological Agency (JMA), Tokyo, Japan*
[3]*Meteorological Research Institute (MRI), Tsukuba, Japan*
[4]*Yokohama National University, Yokohama, Japan*

Abstract

This study examined the diurnal cycles of brightness temperature (TB) and upper-level horizontal winds associated with tropical cyclones (TCs) over the western North Pacific basin, making use of data retrieved from geostationary-satellite (Himawari-8) observations that exhibited unprecedented temporal and spatial resolutions. The results of a spectral analysis revealed that diurnal cycles prevail in TB variations over the outer regions of TCs (300−500 km from the storm center). The dominance of the diurnal cycle was also found in variations in the radial wind (Vr) in intensive TCs, although there was no dominant cycle in tangential wind variation. In addition, coherence spectra demonstrated that the diurnal cycles of TB and Vr are significantly coupled in intensive TCs. The migration speed of TB and Vr anomalies exceeded the time-mean Vr, and it was speculated that diurnal cycle signals propagate (i.e., are not advected) toward the outer regions of TCs.

(**Citation**: Fukuda, K., K. Yasunaga, R. Oyama, A. Wada, A. Hamada, and H. Fudeyasu, 2020: The diurnal cycle of clouds in tropical cyclones over the western North Pacific basin. *SOLA*, **16**, 109−114, doi:10.2151/sola.2020-019.)

1. Introduction

A tropical cyclone (TC) is a storm that develops over tropical or subtropical oceans with sufficiently warm sea surface temperatures. It is characterized by a low-pressure center, intense winds, and heavy rainfall. It is also accompanied by horizontally-extended areas of cirrus cloud, which are referred to as a "cirrus canopy" (e.g., Merritt and Wexler 1967). Cirrus cloud generally forms from the outflow of TC convection and its extension, therefore, is considered to be closely related to TC intensity.

Numerous previous studies have pointed out that cirrus cloud coverage associated with TCs shows a diurnal cycle (e.g., Browner et al. 1977; Muramatsu 1983; Lajoie and Butterworth 1984; Kossin 2002; Dunion et al. 2014; Wang et al. 2019). Using infrared imagery archive of TCs, Kossin (2002) found that diurnal oscillation of the cirrus canopy was evident over 300 km from the center of TCs, although it was weak near the storm center. Examining the evolution of the diurnal cycle in major North Atlantic TCs from 2001 to 2010, Dunion et al. (2014) documented that cyclical pulses in the infrared cloud field regularly propagate radially outward from the TC center, and that diurnal signals are especially prominent a few hundreds of kilometers (200−300 km) away from the circulation center.

Several issues relating to diurnal variations in cirrus cloud extension in TCs remain unresolved. For example, it is recognized that not all TCs show a prominent diurnal cycle, but the reason for this is not understood. In addition, previous studies by Kossin (2002) and Dunion et al. (2014) focused exclusively on Atlantic storms or eastern Pacific storms. Our knowledge of the TC diurnal cycle over the western North Pacific (WNP) basin is limited, even though the WNP is the area where TCs are most frequently generated (e.g., Peduzzi et al. 2012). Furthermore, relationships between cirrus cloud and dynamic fields have not been adequately documented on the basis of observational data, while changes in maximum wind velocity in TCs statistically depend on the local time (e.g., Yaroshevich and Ingel 2013). From a technical point of view, previous studies analyzed observations at a relatively lower time interval of three hours, and it is likely that the results were contaminated by higher-order harmonics due to aliasing.

To develop a more complete understanding of the TC diurnal cycle, therefore, the current study employs datasets with higher temporal and spatial resolutions from a new generation of Japanese geostationary meteorological satellites (Himawari-8) and focuses on TCs over the WNP basin. It should be also emphasized that atmospheric motion vectors (AMVs) derived from images taken by Himawari-8 are included in the analysis, which will be described in the next section.

2. Data and methodology

2.1 Data description

In order to examine the diurnal cycle of upper-level cirrus clouds associated with TCs, the present study used observational products from Himawari-8 and the Regional Specialized Meteorological Center (RSMC) Tokyo best track dataset for the WNP basin.

Himawari-8 started routine operations on 7 July 2015, at 140.7°E. The Himawari-8 imager contains 16 spectral bands, and full-disk images are obtained every 10 min. The spatial resolution of the infrared band is about 2 km. A more complete description of Himawari-8 can be found in Bessho et al. (2016). Regularly-gridded brightness temperature (TB) datasets were provided by the Center for Environmental Remote Sensing (CEReS) at Chiba University. In order to determine cirrus cloud variations in TCs, TBs estimated from 10.4-μm-wavelength-band (band 13) were analyzed.

AMVs are derived by tracking clouds and water vapor patterns in successive (geostationary) satellite images. Retrieval methods for AMVs were developed in the early 1960s (e.g., Menzel 2001), and are being still updated through advanced sensor technologies and/or the adoption of new algorithms (e.g., Velden et al. 2005). AMVs provide unique information for TC analysis and monitoring, even though vertical distributions of AMV datasets are biased in the upper level (e.g., Oyama et al. 2016; Oyama 2017; Oyama et al. 2018). The present investigation used AMVs which were retrieved every 10 min from Himawari-8 TC target observations with a time interval of 5 min (Bessho et al. 2016; Oyama et al. 2018). The retrieval scheme was developed by the Meteorological Satellite Center of the Japan Meteorological Agency, and

---

Table 1. 2016−2017 major TC cases utilized in this study. In the table, axisymmetricity is defined as a ratio of the longest and shortest radiuses of the wind speeds of 30 knots, when a TC reaches the lifetime minimum pressure. R50 and R30 indicate the longest radiuses of the wind speeds of 50 and 30 knots at the peak time of the TCs. All variables are derived from RSMC Tokyo best track data.

	JMA TC No.	TC Name	Lifetime Max MSW [knot]	Lifetime Min. Pressure [hPa]	Axisymmet-ricity	R50 [km]	R30 [km]
1	1601	Nepartak	110	900	1.00	111	444
2	1605	Omais	60	975	0.65	333	695
3	1606	Conson	45	985	0.43	0	648
4	1607	Chanthu	55	980	0.67	222	389
5	1610	Lionrock	90	940	0.60	222	648
6	1612	Namtheun	70	955	0.67	56	167
7	1614	Meranti	120	890	0.63	130	444
8	1616	Malakas	95	930	0.80	111	444
9	1617	Megi	85	945	0.74	259	602
10	1618	Chaba	115	905	0.80	111	444
11	1619	Aere	60	975	0.67	56	222
12	1620	Songda	100	925	0.80	111	333
13	1621	Sarika	95	935	1.00	111	389
14	1626	Nock-ten	105	915	0.50	74	333
15	1702	Merbok	55	985	0.80	74	185
16	1703	Nanmadol	55	985	0.60	37	222
17	1704	Talas	50	985	1.00	0	389
18	1705	Noru	95	935	1.00	111	389
19	1712	Banyan	80	955	1.00	56	222
20	1713	Hato	75	965	0.50	93	333
21	1714	Pakhar	55	985	0.67	56	556
22	1715	Sanvu	80	955	1.00	167	926
23	1718	Talim	95	935	1.00	204	556
24	1721	Lan	100	915	1.00	389	833
25	1722	Saola	60	975	0.78	167	556
26	1723	Damrey	70	970	1.00	130	500
27	1724	Haikui	40	998	0.50	0	222

a detailed description of the algorithm can be found in Shimoji (2014). AMVs in the range 100−200 hPa levels were selected for analysis in this study in view of the quality and the amount of data available at these levels. It is able to be assumed that the levels of clouds and winds coincide with each other, since cloud top in the TC usually reaches the tropopause layer and AMVs are retrieved from sequence images of TB.

RSMC Tokyo best track data cover the period from 1951 to the present and contain 6-hourly measurements of different dimensions of TCs, although the time interval becomes shorter when a TC approaches or makes landfall on Japan: 3 hours or 1 hour. These measurements include the central pressure (Pc), the geographical location of the center, size, grade, 10-min maximum sustained wind (MSW), and longest radius of TCs. The time interval of the best track data is much longer than that of Himawari-8 retrievals (10 min), and variables associated with TCs are linearly interpolated to match the nominal time. The local standard time (LST) of TCs is determined by the location of the TC center with the lowest Pc.

2.2 Analysis method

In the present study, 27 out of 53 TCs traced by Himawari-8 target observations in 2016 and 2017 were analyzed. Short-lived and weak TCs were excluded (Table 1). We were interested in the inherent axisymmetric structures of TCs and their variations which are irrelevant to the environmental flows (e.g., Yasunaga et al. 2016). First, therefore, gridded data of TB and (radial and tangential) winds were azimuthally averaged for annuli of 20 km in radius from the TC center to a distance of 600 km. From the time series of these axisymmetric components at each radius, a 2-day-long segment was sampled for each TC in order to match the resolution of the frequency, since the longevity of TCs is different. The segment was detrended and tapered to zero over the first and last 4.5 hours. Finally, power spectra were computed for each sample, making use of fast Fourier transform algorithms,
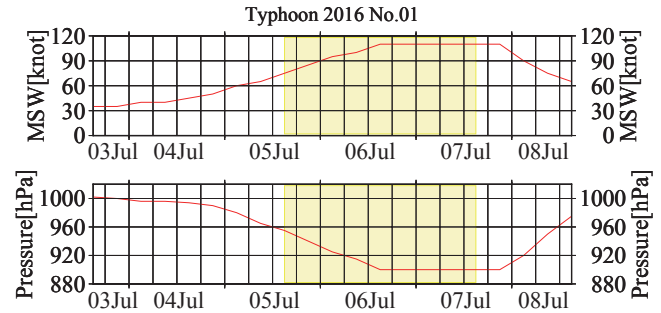

Fig. 1. Evolutions of the MSW (upper) and Pc (lower) of TC 1601 (red line). The period sampled for the calculation of power spectra is shaded in yellow. TB changes associated with the MSW and Pc evolutions are shown in Fig. 5.

and were averaged over all samples after normalization with the sum of the spectra over all frequencies (or variances). The number of samples was limited, and normalization was required to avoid emphasizing the characteristics of a specific TC. The statistical significance of the spectral peak was evaluated, assuming that the power spectrum is distributed according to the chi-square distribution, i.e., a peak was considered to be statistically significant if the 90% confidence interval of the peak exceeded the 90% confidence range on both sides (or at adjacent frequencies).

The present study focused on the diurnal cycle of the developing and mature stage of a TC, and the 2-day-long segment was centered on the time when a TC reached its maximum MSW or minimum Pc (Fig. 1). The duration of the segment (2 days) is short and might not represent the ideal duration for examining the diurnal cycle. However, some TCs decayed within 3 days of formation so it was necessary to choose this duration to secure a sufficient sample size. On the other hand, the results are not sensitive to the duration of the segment (2 days or 3 days).

3. Results

Figure 2 shows the power spectral densities of TB, radial (Vr), and tangential (Vt) winds averaged over the 27 TCs. It can be seen that the power spectra of TB have distinct diurnal cycle peaks over the outer areas of the TC (300−500 km from the storm center), while the diurnal cycle peak is missing near the storm center (Figs. 2a and 2d). In other words, the TB diurnal cycle is prominent in "distant rainbands," which are located over the area beyond 150−200 km from the storm center (e.g., Houze 2010). The dominance of the diurnal cycle in the outer area of a TC can be considered a universal feature, as it occurs over the WNP as well as the North Atlantic (e.g., Kossin 2002; Dunion et al. 2014).

The power spectra of Vr also represent diurnal cycle peaks in the corresponding regions (around 400 km from the TC center), although the signals are much weaker than those of TB (Figs. 2b and 2e). Analyzing dropsonde observations in mature hurricanes, Zhang et al. (2020) documented a clear diurnal signal of boundary layer inflow around a radius of 250−500 km. Therefore, it is indicated that diurnal variations are not merely a passive process in TC clouds, but that dynamic fields, such as horizontal divergence in the upper level, are significantly modulated by the diurnal cycle as well. However, no dominant cycle is evident in the power spectra of Vt (Figs. 2c and 2f), and upper-level circulations appear to be unaffected by the diurnal cycle. It should be also noted that, the diurnal cycle peaks in TB and Vr barely exceed statistically significant levels. This reflects the fact that not all TCs are affected by the diurnal cycle, which provides motivation to investigate the diurnal cycle, further stratifying TCs appropriately.

In Fig. 3, the TCs are categorized into four classes with reference to MSW. The power spectra of the TB display diurnal cycle peaks in almost all categories over those areas located further than 300 km from the storm center, and the peaks are especially sig-
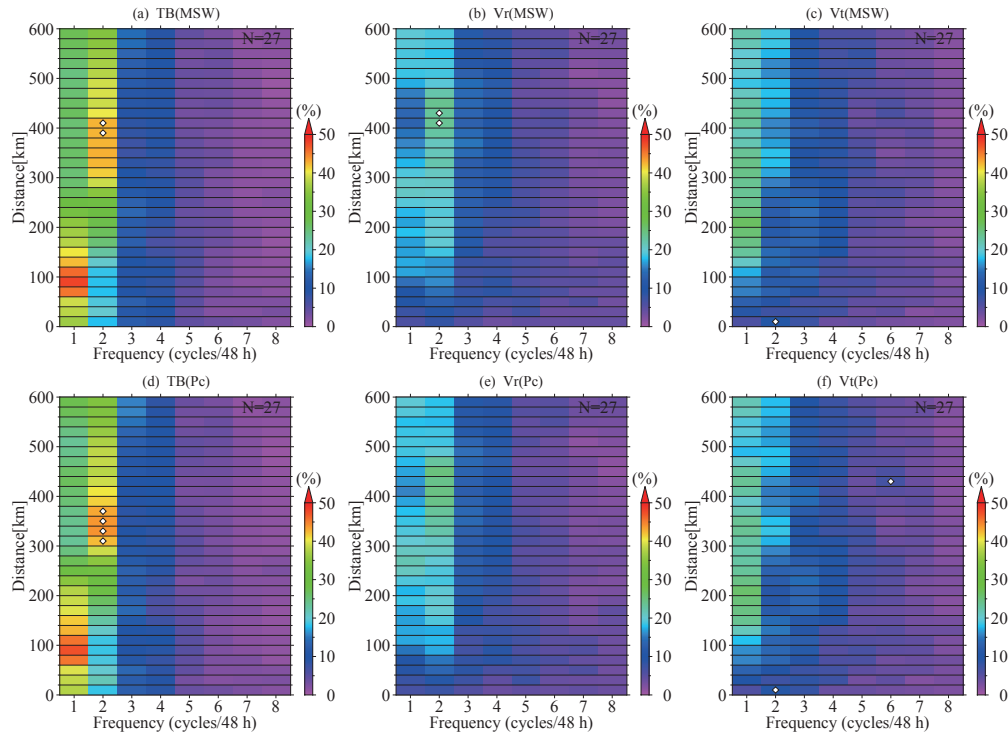
Fig. 2. Power spectra of TB (a and d), Vr (b and e), and Vt (c and f) normalized by the sum of the power spectra over all frequencies (unit: %). For the calculation, 2-day-long (or 48 hours) time series were sampled with reference to the maximum MSW (upper) and minimum Pc (lower) of the TC. The abscissa and ordinate values represent the frequency (unit: cycles per 2 days) and distance of the TC center, respectively (unit: km). A white-colored diamond indicates that the peak is statistically significant (see text).

nificant in TCs with MSWs of 60−80 knots and above 100 knots. Variations in Vr are relatively weak (Figs. 3e−3h), as expected from Fig. 2. However, the TCs with MSWs of 60−80 knots and above 100 knots have prominent diurnal Vr cycles, corresponding to TB variations. Moreover, the diurnal variations in TB and Vr are significantly coherent in the strongest TCs (with MSWs of over 100 knots), while such a significant coherence is absent in other categories (Figs. 3i−3l).

Similar features are also found when TCs are stratified with reference to minimum Pc levels (not shown). On the other hand, one might claim that there are other physical parameters to more clearly distinguish the TCs with and without the diurnal cycle. Therefore, TCs are classified, according to the axisymmetricity at the lifetime minimum pressure, lifetime maximum of the longest radius (See Table 1) and latitude with the longest duration of the TC stay. However, no consistent results are obtained in these stratifications (not shown). As a result, it is suggested that the diurnal cycle is one of the essential features of strong TCs. Furthermore, it is possible that the diurnal cycle over the area of distant rainbands is related to dynamical processes that are responsible for the intensification or maintenance of a TC, although convection in this areas is considered to be relatively free from the constraints of inner-core TC dynamics (Houze 2010).

4. Discussion

It is beyond the scope of the present study to clarify the mechanisms of the diurnal cycle. However, it is worth describing in detail the actual variations in TB and Vr in strong TCs. Figure 4 represents the evolution of the TB and Vr anomalies composited for the TCs with peak MSWs larger than 100 knots (or a minimum Pc lower than 925 hPa), which are included in Figs. 3d, 3h and 3l. The composited variations indicate that TB reaches a minimum at around 15 LST at 300 km from the TC center, and the peak time is delayed with the distance. In addition, it should be emphasized

here that most of the amplitudes of the TB diurnal cycle in the intensive TCs, which fall within about 10 K, are smaller than those estimated for several North Atlantic major hurricanes by previous paper (e.g., Fig. 8 in Dunion et al. 2014), although the phases agree with each other.

Vr variations reach a peak at around 12 LST at 300 km, and the Vr signals gradually propagate to the outer regions as well. It should be noted that the maximum Vr precedes the lowest TB by 3−6 hours at 300−400 km, which is consistent with a phase spectrum where the phase difference between diurnal cycles of TB and Vr is about 60°−70°, or 4.0−4.7 hours (Fig. S1). Although it is difficult to accurately estimate the migration speed of the anomalies from Fig. 4, the phase spectrum between the TB variations at 300 km and 400 km indicates that the diurnal cycle at 400 km lags that at 300 km by about 45°, or 3 hours (not shown). Similarly, the phase difference between the Vr diurnal variations at 300 km and 400 km is estimated to be 30°, or 2 hours (not shown). These phase differences correspond to a migration speed of 9.3− 13.9 m s^{-1}. On the other hand, the time-mean Vr at the corresponding radius composited for strong TCs is about 6−9 m s^{-1}. Therefore, it is speculated that anomalies associated with the diurnal cycle are not advected by the mean wind but propagate toward the outer region of the TC.

Snapshots of TB associated with the first TC of 2016, which exhibits a clear diurnal cycle in its developing and mature stages, are shown in Fig. 5. It is observed that, at 3 LST, deep convective clouds (which are identified by bright white spots) appear around 200 km from the TC center, while cloud cover is minimized at that time. The deep convection reaches a mature stage at 9−12 LST. At 15 LST, the edge of the convection becomes vague, and anvil clouds cover more extended areas (The outer boundary of the anvils exceeds a radius of 300 km). The anvil clouds seem to thin out at 18 LST and decay over the outer region (the area around 300−500 km from the storm center) at 21 LST. Cloud cover contracts at 24 LST and a cloud blob is evident around the TC center (within a radius of 300 km).
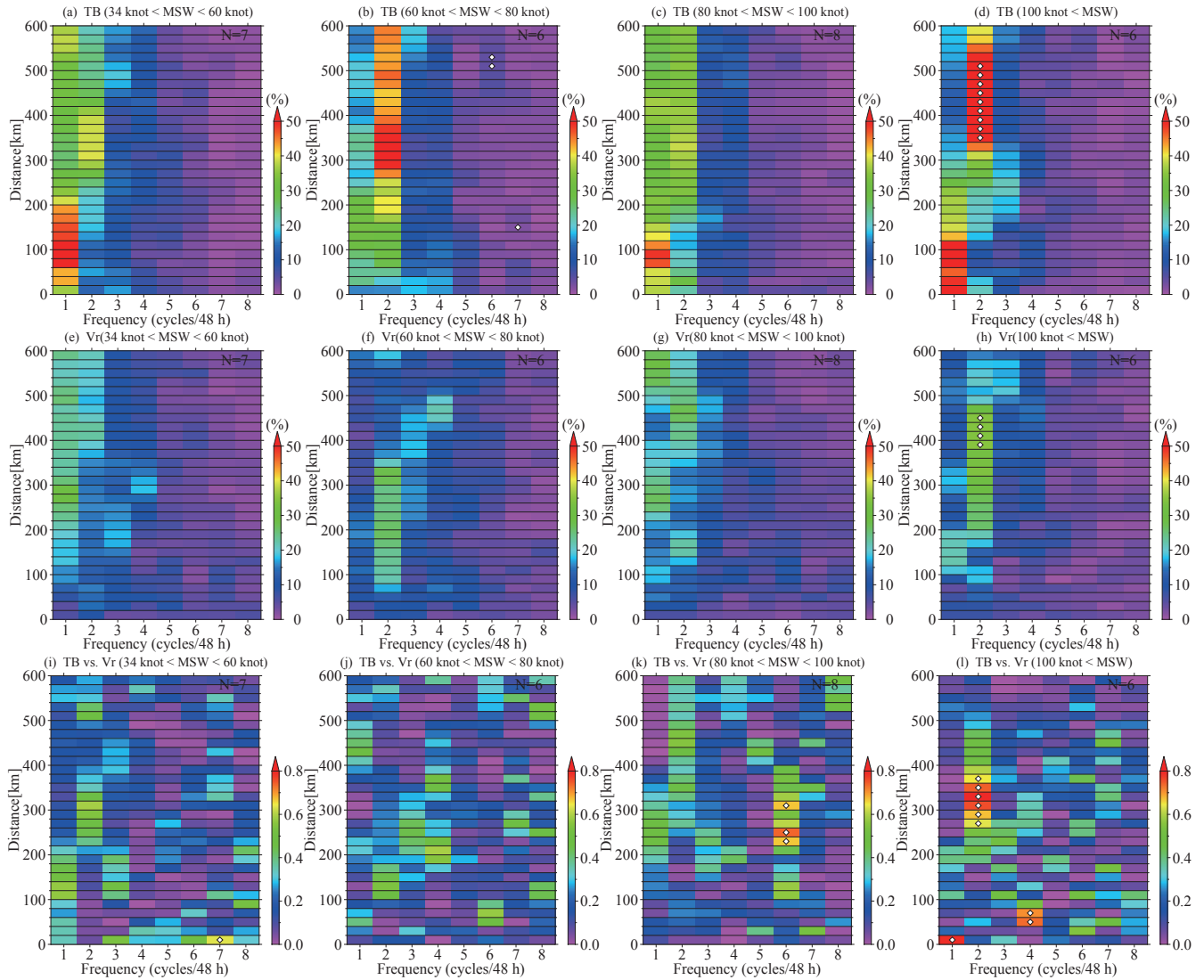
Fig. 3. Power spectra of the TB (upper), the Vr (middle), and the coherence-squared spectrum between TB and Vr (bottom). The power spectra are normalized by the sum of the power spectra over all frequencies (unit: %). TCs are stratified into four classes with reference to the MSW (left: 34 knots < MSW < 60 knots, center left: 60 knots < MSW < 80 knots, center right: 80 knots < MSW < 100 knots, right: 100 knots < MSW), and the sample number is shown in the upper right corner of each panel. The abscissa and ordinate values represent the frequency (unit: cycles per 2 days) and distance of the TC center (unit: km), respectively. A white-colored diamond in the upper and middle panels indicates that the peak is statistically significant (see text), while a white-colored diamond in the bottom panels shows that the coherence exceeds 0.61 (which is statistically significant at the 99% level with 12 degrees of freedom).
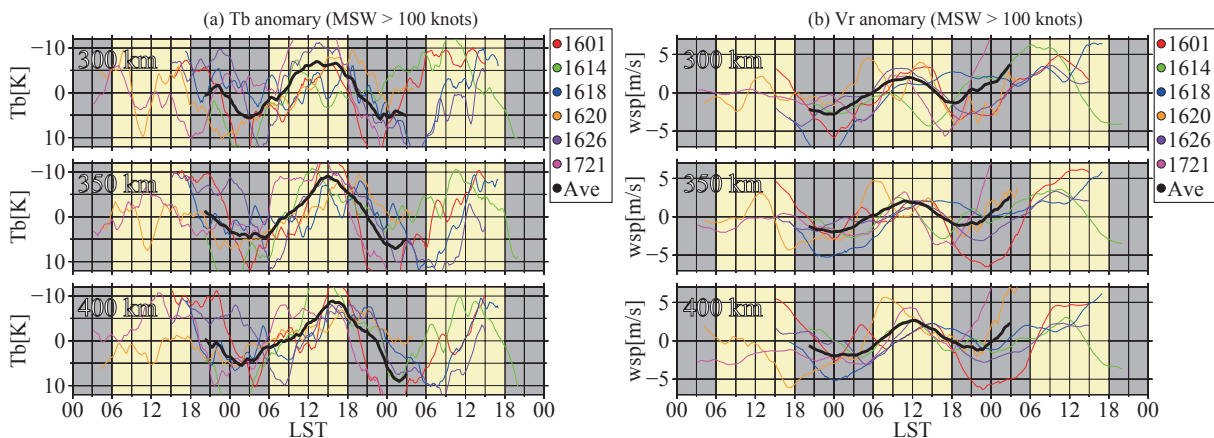

Fig. 4. Evolution of the (a) TB and (b) Vr anomalies composited for the TCs with a maximum MSW larger than 100 knots. The upper, middle, and bottom panels represent the composites (thick solid line) at the distance of 300 km (upper), 350 km (middle), and 400 km (bottom) from the circulation center. Anomalies are calculated by subtracting the time-mean. Thin solid lines in the panels indicate variations of each TC at a given distance.

00LST 06 Jul. 2016
Center : (132.70 , 17.55)
Pressure : 932[hPa]
MSW : 90[kt]
Long Radius : 388[km]
Short Radius : 277[km]

03LST 06 Jul. 2016
Center : (131.90 , 18.00)
Pressure : 925[hPa]
MSW : 95[kt]
Long Radius : 444[km]
Short Radius : 277[km]

06LST 06 Jul. 2016
Center : (131.00 , 18.35)
Pressure : 920[hPa]
MSW : 97[kt]
Long Radius : 444[km]
Short Radius : 277[km]

09LST 06 Jul. 2016
Center : (130.10 , 18.70)
Pressure : 915[hPa]
MSW : 100[kt]
Long Radius : 444[km]
Short Radius : 277[km]

12LST 06 Jul. 2016
Center : (129.25 , 19.10)
Pressure : 907[hPa]
MSW : 105[kt]
Long Radius : 444[km]
Short Radius : 277[km]

15LST 06 Jul. 2016
Center : (128.40 , 19.50)
Pressure : 900[hPa]
MSW : 110[kt]
Long Radius : 444[km]
Short Radius : 277[km]

18LST 06 Jul. 2016
Center : (127.70 , 19.80)
Pressure : 900[hPa]
MSW : 110[kt]
Long Radius : 416[km]
Short Radius : 333[km]

21LST 06 Jul. 2016
Center : (127.00 , 20.10)
Pressure : 900[hPa]
MSW : 110[kt]
Long Radius : 388[km]
Short Radius : 388[km]

00LST 07 Jul. 2016
Center : (126.30 , 20.40)
Pressure : 900[hPa]
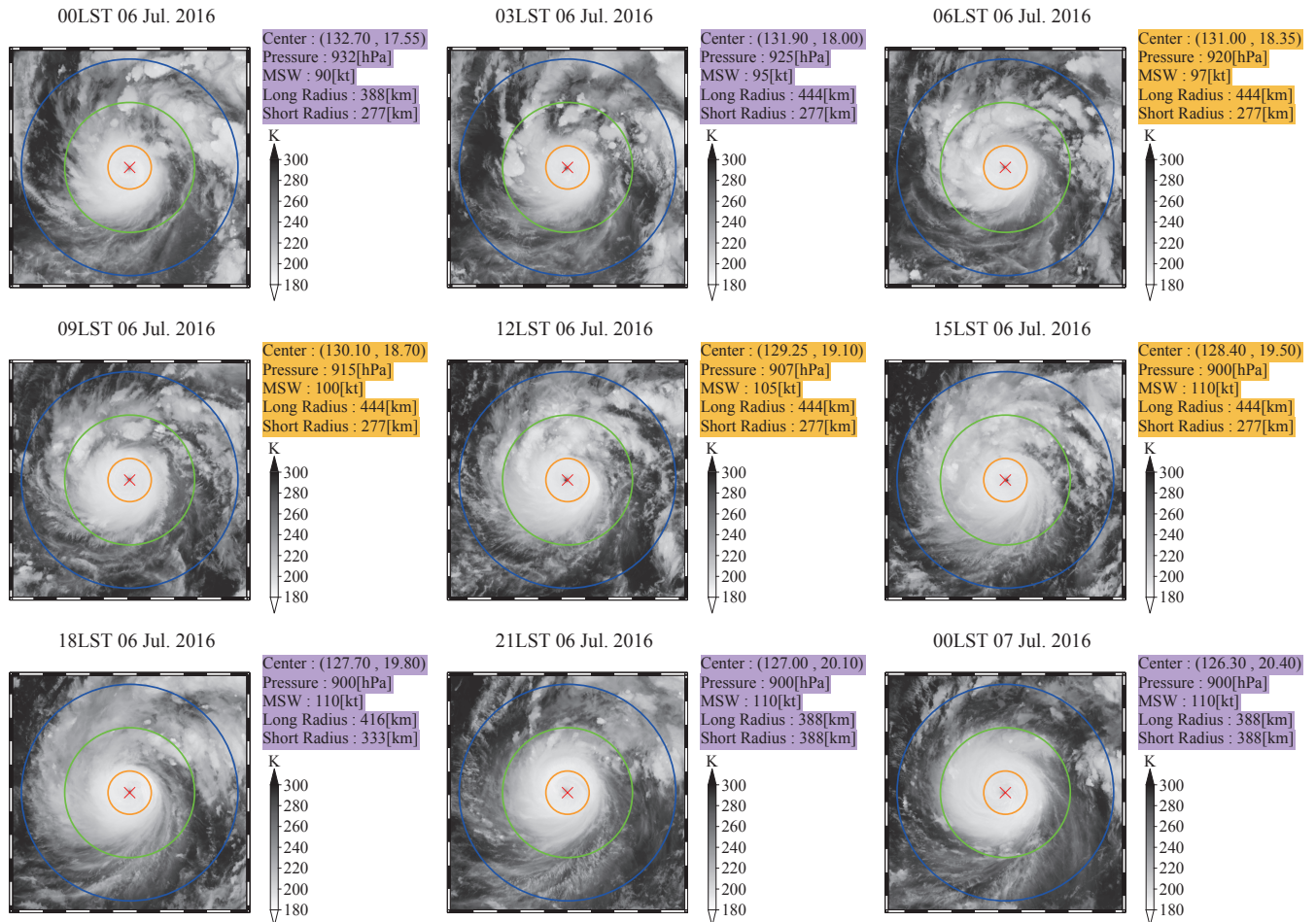MSW : 110[kt]
Long Radius : 388[km]
Short Radius : 388[km]

Fig. 5. TB Snapshots of TC 1601 (from 00 LST on July 6 to 00 LST on July 7). The time interval of the snapshots is 3 hours. Orange, green, and blue circles represent radii of 100 km, 300 km, and 500km from the TC center, respectively. The geographical location and pressure of the TC center, MSW, longest radius, and shortest radius of 30 knots are given in the upper right section of each panel, and the background color of the annotations indicates daytime (orange) or nighttime (purple). The locations, central pressure, MSW and radiuses in the annotations are linearly interpolated from the RSMC Tokyo best track data (see text).

Although these snapshot sequences might include features of the spontaneous development, we speculate that the diurnal cycles of convective activity and the associated anvil in the outer band of a TC are the fundamental processes assisting in the intensification or maintenance of a TC. However, further investigations are required to confirm this speculation.

5. Conclusion and summary

This study examined diurnal cycles of the TB and upper-level winds associated with TCs over the WNP basin, making use of Himawari-8 images of unprecedented temporal and spatial resolution. The results of a spectral analysis revealed that the diurnal cycle of the TB prevails in the areas beyond 300 km from the TC center, while diurnal cycle signals are absent near the storm center. The dominance of the diurnal cycle was also found in Vr variations in intensive TCs. In addition, the coherence spectra between TB and Vr demonstrated that diurnal variation is not merely a passive process in a TC, but that diurnal cloud cycles and horizontal divergence in the upper level are significantly coupled in intensive TCs. On the other hand, there is no dominant cycle in Vt variations. Composites of TB and Vr variations in intensive TCs illustrated that the lowest TB emerges around 15 LST, and the TB minimum lags a Vr peak by 3−6 hours. The migration speed estimated from the phase spectra significantly exceeds the time-mean Vr. Therefore, it is speculated that diurnal cycle signals propagate (i.e., are not advected).

The results obtained here are largely consistent with those from previous studies. However, the present study is the first to statistically examine the diurnal cycle of TCs over the WNP basin. Another novel point is that AMV products derived from Himawari-8 observations were included in the analysis in this study. Various weather forecast centers in the world rely on the Dvorak technique (Dvorak 1975) to estimate TC intensity. In some cases, however, the Dvorak technique ignores rapid developments in TC intensity within several hours (e.g., Kishimoto et al. 2013). On the other hand, Oyama and Wada (2019) demonstrated, through numerical experiments using a non-hydrostatic model, that TC warm core intensification is associated with the diurnal cycle and other short-timescale variations in TC convection. Considering these facts, the results of the present study provide a basis for better estimation of TC intensity (and an improvement on the Dvorak technique). However, the physical mechanisms responsible for the diurnal cycle and its role in the intensification and/or maintenance of TCs were left unresolved and should be clarified in future studies. The following questions might be keys to address those issues; why the tangential wind has no dominant cycles, and what kind of clouds are responsible for the diurnal cycle (eyewall, rainbands, or local convection).

Storm sizes are different among the TCs, and normalization by a certain length scale might be useful to highlight the critical distance where the diurnal cycle dominates. However, there are several options to determine the scale of a TC (e.g., R50 and R30

in Table 1), and it is difficult to select the most adequate parameter for the present purpose. Therefore, such normalization processing is also left for the future study.

Acknowledgments

Edited by: T.-Y. Koh

References

Bessho, K., and co-authors, 2016: An introduction to Himawari-8/9 −Japan's new-generation geostationary meteorological satellites. *J. Meteor. Soc. Japan. Ser. II*, **94**, 151−183, doi: 10.2151/jmsj.2016-009.

Browner, S. P., W. L. Woodley, and C. G. Griffith, 1977: Diurnal oscillation of the area of cloudiness associated with tropical storms. *Mon. Wea. Rev.*, **105**, 856−864, doi:10.1175/1520-0493(1977)105<0856:DOOTAO>2.0.CO;2.

Dunion, J. P., C. D. Thorncroft, and C. S. Velden, 2014: The tropical cyclone diurnal cycle of mature hurricanes. *Mon. Wea. Rev.*, **142**, 3900−3919, doi:10.1175/MWR-D-13-00191.1.

Dvorak, V. F., 1975: Tropical cyclone intensity analysis and forecasting from satellite imagery. *Mon. Wea. Rev.*, **103**, 420−430, doi:10.1175/1520-0493(1975)103<0420:TCIAAF>2.0.CO;2.

Houze, R. A., 2010: Clouds in tropical cyclones. *Mon. Wea. Rev.*, **138**, 293−344, doi:10.1175/2009MWR2989.1.

Kishimoto, K., M. Sasaki, and M. Kunitsugu, 2013: Cloud grid information objective dvorak analysis (CLOUD) at the RSMC Tokyo - Typhoon Center, RSMC Tokyo. *Typhoon Cent. Tech. Rev.*, **15**, 1−15.

Kossin, J. P., 2002: Daily hurricane variability inferred from GOES infrared imagery. *Mon. Wea. Rev.*, **130**, 2260−2270, doi:10.1175/1520-0493(2002)130<2260:DHVIFG>2.0.CO;2.

Lajoie, F. A., and I. J. Butterworth, 1984: Oscillation of high-level cirrus and heavy precipitation around Australian region tropical cyclones. *Mon. Wea. Rev.*, **112**, 535−544, doi:10.1175/1520-0493(1984)112<0535:OOHLCA>2.0.CO;2.

Menzel, W. P., 2001: Cloud tracking with satellite imagery: From the pioneering work of Ted Fujita to the present. *Bull. Amer. Meteor. Soc.*, **82**, 33−48, doi:10.1175/1520-0477(2001)082<0033:CTWSIF>2.3.CO;2.

Merritt, E. S., and R. Wexler, 1967: Cirrus canopies in tropical storms. *Mon. Wea. Rev.*, **95**, 111−120, doi:10.1175/1520-0493(1967)095<0111:CCITS>2.3.CO;2.

Muramatsu, T., 1983: Diurnal variations of satellite-measured TBB areal distribution and eye diameter of mature typhoons. *J. Meteor. Soc. Japan. Ser. II*, **61**, 77−90, doi:10.2151/jmsj1965.61.1_77.

Oyama, R., 2017: Relationship between tropical cyclone intensification and cloud-top outflow revealed by upper-tropospheric atmospheric motion vectors. *J. Appl. Meteor. Climatol.*, **56**, 2801−2819, doi:10.1175/JAMC-D-17-0058.1.

Oyama, R., and A. Wada, 2019: The relationship between convective bursts and warm-core intensification in a nonhydrostatic simulation of typhoon lionrock (2016). *Mon. Wea. Rev.*, **147**, 1557−1579, doi:10.1175/MWR-D-18-0457.1.

Oyama, R., A. Wada, and M. Sawada, 2016: Intensification of Typhoon Danas (1324) captured by MTSAT upper tropospheric atmospheric motion vectors. *SOLA*, **12**, 135−139, doi:10.2151/sola.2016-029.

Oyama, R., M. Sawada, and K. Shimoji, 2018: Diagnosis of tropical cyclone intensity and structure using upper tropospheric atmospheric motion vectors. *J. Meteor. Soc. Japan. Ser. II*, **96B**, 3−26, doi:10.2151/jmsj.2017-024.

Peduzzi, P., B. Chatenoux, H. Dao, A. De Bono, C. Herold, J. Kossin, F. Mouton, and O. Nordbeck, 2012: Global trends in tropical cyclone risk. *Nat. Climate Change*, **2**, 289−294, doi:10.1038/nclimate1410.

Shimoji, K., 2014: Motion tracking and cloud height assignment methods for Himawari-8 AMV. *12th International Winds Workshop*, Copenhagen, Denmark.

Velden, C., and co-authors, 2005: Recent innovations in deriving tropospheric winds from meteorological satellites. *Bull. Amer. Meteor. Soc.*, **86**, 205−224, doi:10.1175/BAMS-86-2-205.

Wang, X., H. Iwabuchi, and N. Takahashi, 2019: Characteristics of diurnal pulses observed in Typhoon Atsani using retrieved cloud property data. *SOLA*, **15**, 137−142, doi:10.2151/sola.2019-025.

Yaroshevich, M. I., and L. K. Ingel, 2013: Diurnal variations in the intensity of tropical cyclones. *Izv. Atmos. Ocean. Phys.*, **49**, 375−379, doi:10.1134/S0001433813040117.

Yasunaga, K., T. Miyajima, and M. Yamaguchi, 2016: Relationships between tropical cyclone motion and surrounding flow with reference to longest radius and maximum sustained wind. *SOLA*, **12**, 277−281, doi:10.2151/sola.2016-054.

Zhang, J. A., J. P. Dunion, and D. S. Nolan, 2020: In situ observations of the diurnal variation in the boundary layer of mature hurricanes. *Geophys. Res. Lett.*, **47**, 2019GL086206, doi:10.1029/2019GL086206.